3D MODELLING OF BI-STEEL STRUCTURES SUBJECT TO FIRE

CHAOMING YU[1], Z. HUANG[2], I. W. BURGESS[3], R. J. PLANK[4]

ABSTRACT

This research is aimed at analysing the performance in fire of Bi-Steel panels used predominantly as compressive structures, such as building cores. In this paper, thermal behaviour of the Bi-Steel panel is analyzed, and a series of parametric studies are carried out. A further object of this research is to develop a non-linear procedure for modelling of the structural behaviour of Bi-Steel panels subject to fire. In this procedure, the Bi-Steel panel has been represented as an assembly of steel plates, a concrete core and steel bar connectors, using three-dimensional brick elements, and both material and geometric non-linearities are considered.

1. INTRODUCTION

Traditional steel-concrete-steel double-skin composite construction (DSC) consists of a core of concrete sandwiched between two thin steel plates. The overlapping steel studs, which act as transverse shear reinforcement, transfer the normal and shear forces between the concrete and steel plates [1]. However, since each shear stud in DSC is only connected to one steel plate, there is no continuous bond maintained between the concrete core and the plates. Lack of full composite action could be one reason for the failure of this type of structure.

The Bi-Steel panel, which is composed of two steel facing plates connected by an array of transverse friction-welded shear connectors and filled with concrete, was developed

[1] PhD student, Department of Civil and Structural Engineering, University of Sheffield, S1 3JD, UK.
Email: c.yu@sheffield.ac.uk

[2] Lecturer, Department of Civil and Structural Engineering, University of Sheffield, S1 3JD, UK.

[3] Professor, Department of Civil and Structural Engineering, University of Sheffield, S1 3JD, UK.

[4] Professor, School of Architectural Studies, University of Sheffield, S10 2TN, UK.

by Corus Group Ltd from DSC. In this structure, the steel faceplates provide resistance to both in-plane and bending forces. This is because the faceplates are equivalent to a significant area of steel reinforcement, and are in the optimal position to maximise bending resistance. The steel bar connectors are multi-functional, and provide shear reinforcement to the concrete core. They carry longitudinal shear flow between the faceplates and the concrete core, prevent buckling of the faceplates, and provide a permanent tie between the front and rear plates. Concrete provides resistance to compressive and shear forces. Normally, it is placed within the voids after panel erection has been finished on site, with the steel faceplates acting as formwork, enabling high concreting pressures to be sustained during construction. When faceplates connect to one another and to the concrete core, the entire Bi-Steel section behaves as a single composite rather than as individual elements. This structural system has several useful features, including enhanced blast and fire resistance, thickness reduction in core walls, leak resistance, and optimization of site work and site time[2].

At ambient temperature, the structural behaviour of Bi-Steel panels has been studied during recent years. This work has focused on analyzing the shear and tensile performance of the steel bar connectors, and the composite action between the concrete core and the steel faceplates [3-6]. Experimental testing and finite element methods have been used in these studies. The following structural characteristics have been found:

1) The Bi-Steel panel has significant shear capacity when it is subject to push-out loading. The shear strength is affected by several parameters, including plate spacing, connector spacing and shear connector diameter. A smaller connector spacing in the Bi-Steel panel produces increased slip and a lower failure load [3].
2) The shear strength of a Bi-Steel panel with thin faceplates is governed by the strength of the plates. The shear strength of a panel with thick plates is governed primarily by the fracture strength of the friction weld [4].
3) The Bi-Steel panel has high ductility and deformation capacity.

However, there have been few studies of the behaviour in fire of Bi-Steel components or structures. At elevated temperatures, the capacity of Bi-Steel panels for carrying load will be reduced. The strength and stiffness of both steel and concrete are reduced by the high temperatures, and this combines with the curvatures and stresses caused by the thermal gradient, which reduce the buckling resistance of the steel plates. Hence, the structural characteristics and stress situations within a Bi-Steel panel in fire can be very complicated.

In the building fire resistance context, it is necessary to do some detailed research in this field. For Bi-Steel panels, the calculation of fire resistance involves the determination of temperature distribution, deformation and stress under various types of loading.

2. THERMAL ANALYSIS

2.1 3D heat transfer simulation

The finite element analysis software ABAQUS was used to generate temperature information. A Bi-Steel panel without additional fire protection, exposed to the standard ISO 834 fire, is presented for thermal analysis. Material properties are illustrated in Table 1.

Table 1 Summary of material properties used in analysis

Component	Dimension L×H×t / diameter (mm)	Density (kg/m^3)	Material grade	Strength (MPa)	Moisture content by weight (%)
Steel faceplate	200×200×15	7850	S355JR	355	
Steel bar connector	25	7850	070M20	370	
Concrete	200×200×200	2400	C45	45	5

The emissivity of the fire is taken as 0.8, and the coefficient of heat transfer by convection is 25 W/m^2·K [7]. Other values of thermal properties, such as the specific heats and the thermal conductivities of both steel and concrete, are given in EN 1994-1-2 [8].

Because of the inherent symmetry of the case, only a cuboid of Bi-Steel was considered here (see Fig. 1). Due to the basic theory of the finite element method, the model required is a mesh of nodes and elements. 3D diffusive heat-transfer solid elements (DC3D8) were chosen to represent the steel and the concrete within ABAQUS. Since the mesh density of elements has an influence on the accuracy of calculation, some sensitivity analyses had to be undertaken to determine the appropriate mesh of elements. On the basis of the results of the sensitivity analysis, the Bi-Steel model was divided into 729 DC3D8 elements and 1000 nodes. For the sake of convenience, the steel bar connector was also represented by a column of 8-node solid elements, with cross-section equal to the real area.

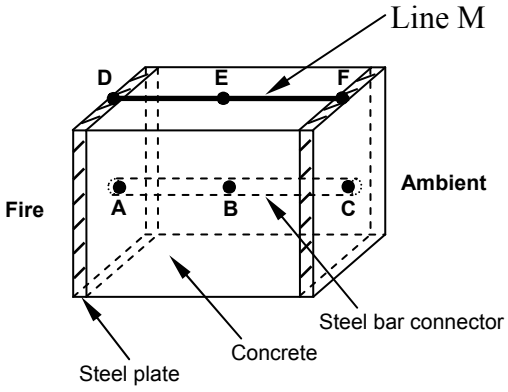

Fig. 1 – Typical 3D Bi-Steel model

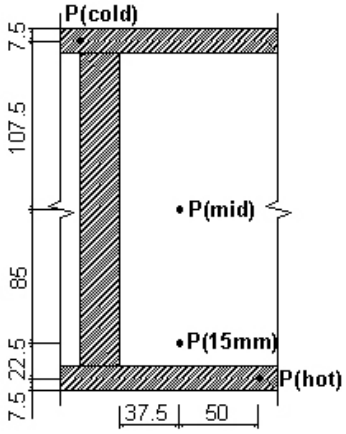

Fig. 2 – Key points used in heat transfer analysis

Uncoupled heat transfer analysis, which calculates the temperature field including the effects of conduction, forced convection and boundary radiation, but without any knowledge of the stress and deformation state being studied, was chosen as the analysis type defined within ABAQUS. Results generated were compared with the temperature values provided by the 'Bi-Steel Design and Construction Guide' (referred to as The Bi-Steel Guide in the following parts of this paper). The compared key positions are shown in Fig. 2. As the following charts (Figs. 3 to 6) show, at the point *P(hot)*, the histories of steel temperatures obtained from ABAQUS and The Bi-Steel Guide are quite similar (Fig. 3). At the position *P(mid)*, concrete temperatures predicted by the two models are slightly different (Fig. 4).

However, at points *P(cold)* and *P(15mm)* (which is 15mm away from the heated faceplate), there are significant (up to 66%) differences in temperature between ABAQUS and The Bi-Steel Guide (Figs. 5 and 6). This inconsistency might be induced by the different values of thermal properties implied in ABAQUS analysis and The Bi-Steel Guide. In the latter case their values are not specified, even though they are based on EN 1994-1-2. Additionally, from the information provided by The Bi-Steel Guide, it seems likely that only 2D thermal analysis was conducted.

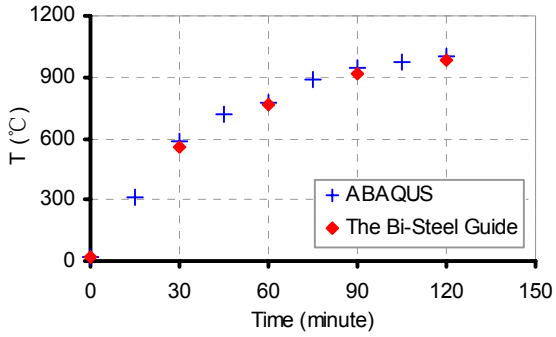

Fig. 3 – Temperatures at *P(hot)*

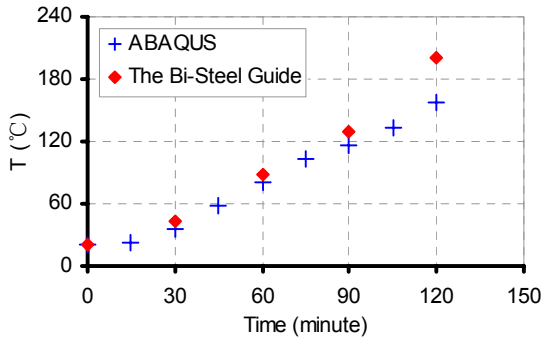

Fig. 4 – Temperatures at *P(mid)*

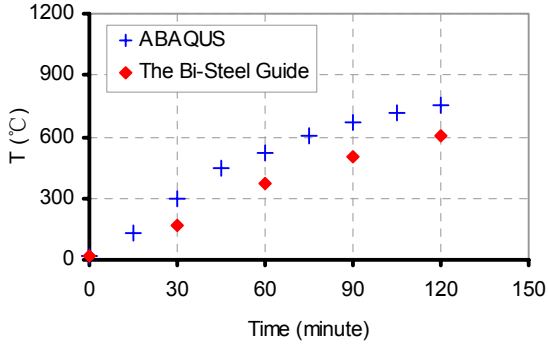

Fig. 5 – Temperatures at *P(15mm)*

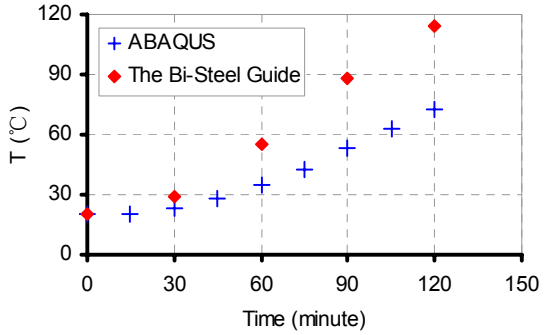

Fig. 6 – Temperatures at *P(cold)*

2.2 Analysis of the influence of thermal parameters

In order to analyze the thermal behaviour of the Bi-Steel panel properly, some parametric studies have been carried out in this research. These have focused on studying the effects of heat flux, concrete moisture content, the emissivity of the fire, and the steel bar connector properties on the temperature distributions of the model.

2.2.1 Effect of heat flux

Since the nature of a real fire depends on the fire load density and ventilation conditions, it is effective to use two extreme constant heat fluxes representing a range of different fire conditions. Here, the higher heat flux employed in this paper is 40,000W/m^2 which was calculated according to the Hydrocarbon fire curve, and the lower is 20,000W/m^2. The temperature distributions along the steel bar connector and the line M (see Fig. 1) at 30 and 60 minutes fire time are plotted in Figs. 7 and 8. The temperature gradient between the

two steel faceplates is very large. Moreover, even with extremely large heat flux, at 60 minutes the temperature of the cold surface is below 40°C.

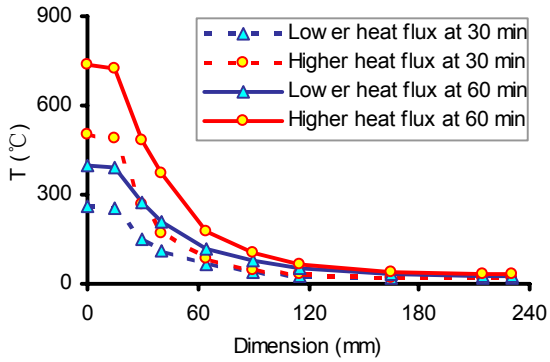

Fig. 7 – Temperature distributions along steel bar connector

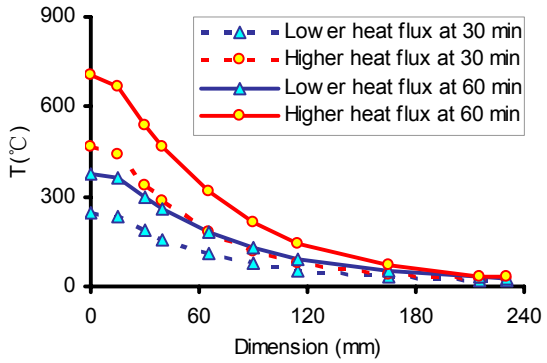

Fig. 8 – Temperature distribution along the line M

2.2.2 Effect of concrete moisture content

Since the moisture content of concrete can affect the peak value of specific heat, the temperature distribution of the model can change with it. In this paper, two values of moisture content (0% and 5% by weight) have been used in analysis. From Figs. 9 and 10 it is evident that the influence of moisture content on the temperature distribution is significant (with up to 45% difference) within the central area of the Bi-steel section, but insignificant within the area close to the hot surface. This is because, at *P(15mm)*, the fire temperature and emissivity have a greater influence on the temperature distribution than the moisture content. Overall, however, the moisture content of concrete is an important factor in the thermal analysis of the Bi-Steel panel.

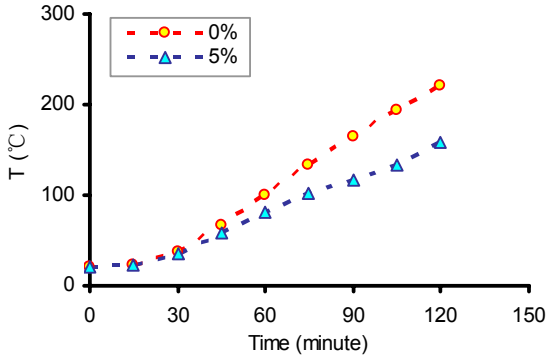

Fig. 9 – Concrete temperature variation at *P(mid)*

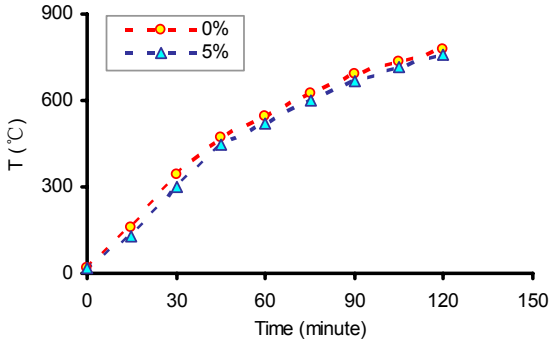

Fig. 10 – Concrete temperature variation at *P(15mm)*

2.2.3 Effect of the emissivity of fire

The emissivity of a fire is a function of the size of the flame and varies between fuel types. Results generated by numerical modelling, in which the emissivity of fire was changed from 0.6 to 0.8, are plotted in Figs. 11 and 12. It can be seen that there is a slightly

larger difference in the temperature variation of the hot steel faceplate (about 10%) than that in the temperature variation of mid-plane concrete (about 5%). Therefore, it is inferred that the fire emissivity is not a significant parameter to this temperature generation analysis.

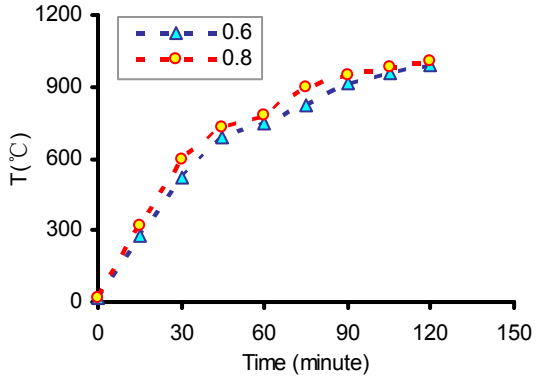

Fig. 11 – Temperatures at *P(hot)*

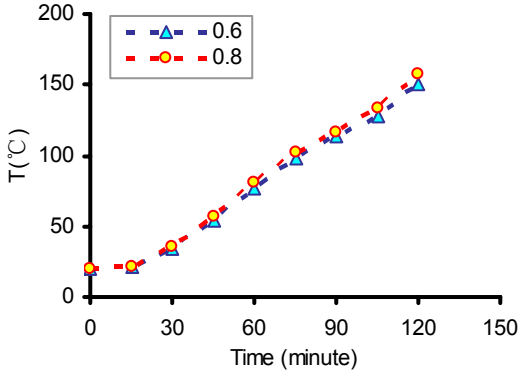

Fig. 12 – Temperatures at *P(mid)*

2.2.4 Effect of steel bar connectors

According to The Bi-Steel Guide, it is not very important to model the temperature gradient accurately at points between the steel faceplates, because the behaviour of the Bi-Steel panel is dominated by faceplate behaviour. Furthermore, the reinforcement ratio in terms of the steel bar connectors is just 7.6% in the 3D model. However, it is necessary to validate whether steel bar connectors can be ignored in finite element analysis.

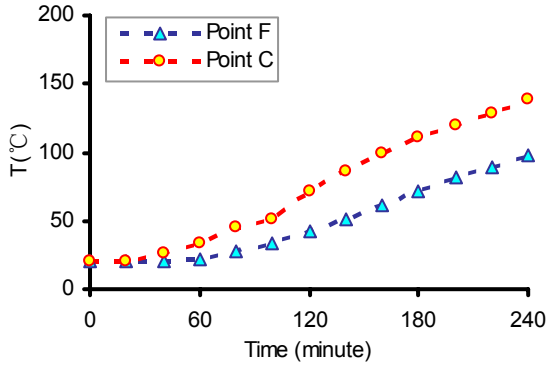

Fig. 13 – Temperatures at cold faceplate

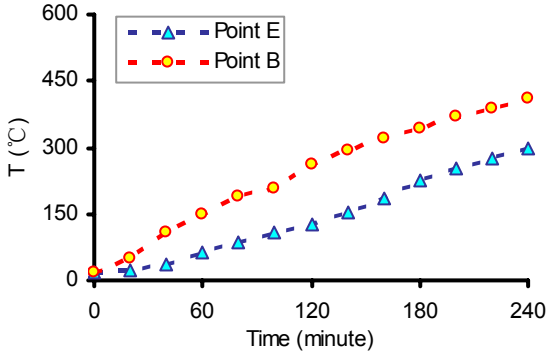

Fig. 14 – Temperatures at mid-bar

Within the analysis, three points A, B and C, whose positions along the steel bar connector are respectively at the hot faceplate, the mid-plane and the cold faceplate, were selected and compared with points D, E and F (see Fig. 1). From plotted results (see Figs. 13, 14 and 15), It can be seen that the temperature values at the compared points with the bar connector included in the model is up

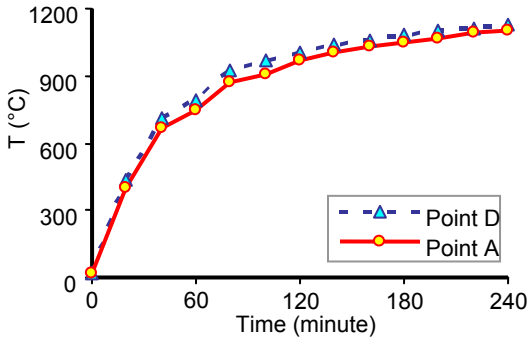

Fig. 15 – Temperatures at hot faceplate

to 106% larger than those without the bar connector included, except for those at the heated faceplate. This is because, at the hot surface, the fire temperature and the emissivity of the fire have a greater influence on the temperature distributions within the Bi-Steel panel. Hence, in the simulation, the steel bar connectors have to be taken into account.

3. NON-LINEAR PROCEDURE FOR STRUCTURAL ANALYSIS

Before moving on to the structural analysis of a Bi-Steel panel at elevated temperature, the simulation program had to be chosen. On consulting literature reviews concerning the use of ABAQUS to model structures at high temperature, it was found that numerical problems were too severe for results to be obtained [9]. In order to confirm this, the author has tested a 3D composite structure under fire conditions in ABAQUS. It may be because the failure criteria used in the elevated-temperature concrete material model of ABAQUS are too inefficient to converge. Thus, in this research, ABAQUS was not adopted to simulate the structural behaviour of Bi-Steel panels in fire.

An in-house finite element program *Vulcan*, which provides slab, beam-column, spring and shear-connector elements, has been developed by the University of Sheffield for 3D modelling of concrete, steel and steel-framed composite structures in fire [10]. However, the Bi-Steel panel is a complicated three-dimensional problem. One- or two-dimensional stress-strain relationships are not adequate to represent the real behaviour of Bi-Steel panels. Hence, a three-dimensional eight-noded brick element had to be developed in order to model Bi-steel properly. Both geometric and material non-linearities were considered. A Newton-Raphson method was applied as the iteration scheme for the solution of the non-linear finite element equations. Some fundamental assumptions of the non-linear approach can be summarized as:

1) The displacements of brick elements may be large, but element extensions and angle changes between elements are small.
2) Each brick element can have a different but uniform temperature. Three-dimensional stress-strain relationships can change independently at every single Gauss point of each element, and there is no slip between elements.
3) In the elastic region, steel is isotropic, which means that the initial mechanical properties are the same in any direction at a material point. Concrete is isotropic, homogenous and elastic before cracking or crushing occurs.
4) Plastic deformations are irreversible and history-dependent. Plastic deformations of steel are hydrostatic-pressure-insensitive, but those of concrete are hydrostatic-pressure-sensitive.
5) The associated flow rule, which defines that the plastic potential surface has the same shape as the yield surface, has been adopted.
6) The plastic behaviour obeys the theory of plasticity, i.e. the stiffness of elastic unloading-reloading does not change with plastic deformations.
7) Concrete, on cooling down to ambient temperature of 20°C after having reached an elevated temperature, does not recover its initial compressive strength.

3.1 Geometrically non-linear brick element

In general, geometric non-linearity occurs when deformations become so large that they introduce additional internal actions. According to a study of the literature, Bathe [11] has set up a series of 3D isoparametric finite element formulations including material linear-elasticity. Hence, the geometrically non-linear brick element was extended to include material non-linearities for modelling of structures in fire.

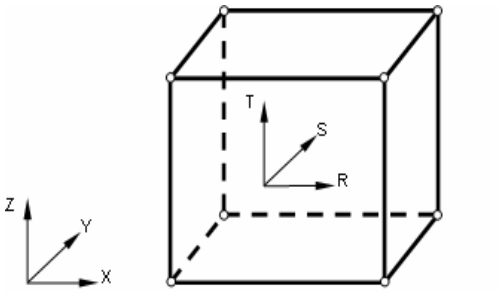

Fig. 16 – 3D eight-noded brick element

In this model, using a Total Lagrangian formulation, the basic static finite element equilibrium equation can be written as

$$({}_0^tK_L + {}_0^tK_{NL}) \cdot \Delta U = {}^{t+\Delta t}R - {}_0^tF \tag{1}$$

where ${}_0^tK_L$ is the linear-strain incremental stiffness matrix; ${}_0^tK_{NL}$ is the non-linear-strain incremental stiffness matrix; U is the vector of increments in the nodal point displacements; ${}^{t+\Delta t}R$ is the vector of externally applied nodal point loads at time $t+\Delta t$; and ${}_0^tF$ is the vector of nodal point forces equivalent to the element stresses at time t. Gaussian numerical integration is used to calculate the stiffness matrix and internal forces. Generally, the appropriate integration order depends on the matrix being evaluated and the specific finite element being considered. Here, a fully integrated 3D eight-noded element integrated at 8 Gauss points (2×2×2) is adopted. In the numerical procedure, the equilibrium relationship must be satisfied throughout the complete history of load application, so that the correct displacements can be obtained.

3.2 Material model

In the developing process of the 3D material model, a key point is to work out the relationship between uniaxial stress-strain curves and 3D stress surfaces. For the sake of convenience, the effective stress and the effective plastic strain are defined for the multi-axial stress state such that the single $(\sigma_{effective}\text{-}\varepsilon_{effective}^{p})$ curve can be calibrated against a uniaxial stress-plastic strain curve [12]. Uniaxial stress-strain curves, which are documented in Eurocode 4 Part 1.2, are referenced and translated into triaxial mechanical models of steel and concrete at different temperatures.

3.2.1 Steel model

The von Mises criterion was chosen as the yield function of steel [12]. It is formed as

$$f(J_2) = J_2 - k^2 = 0 \tag{2}$$

where J_2 is the second invariant of the deviatoric stress tensor. The material constant

$$k = \frac{\sigma_0}{\sqrt{3}} \tag{3}$$

where σ_0 is the uniaxial yield stress. According to the yield function, it can be seen that stress points can freely move on the yield surface which is determined by k. Thus, the determination of the material constant k, which is also called as the yield stress of material in pure shear, is very important in the numerical procedure. At elevated temperature, material degradation occurs. Both yield strength and Young's modulus decrease with increasing temperature. Hence, there is a constant value for k at every single temperature point. In other words, the yield surface is a function depending on different temperature values.

In the linear-elastic stage, the stress-strain relationship is given as Equation (4). Beyond the proportional limit, the stress point enters into elastic-plastic stage. Its relationship changes to Equation (5), and plastic strains are produced by further loading. Since an associated flow rule has been assumed, plastic strain increments can be defined using Equation (6).

$$d\sigma_{ij} = C_{ijkl} \cdot d\varepsilon_{kl} \tag{4}$$

$$d\sigma_{ij} = C_{ijkl}^{ep} \cdot d\varepsilon_{kl} \tag{5}$$

$$d\varepsilon_{ij}^{p} = d\lambda \cdot \frac{\partial f}{\partial \sigma_{ij}} \tag{6}$$

where C_{ijkl} is the tensor of temperature-dependent elastic stiffness; C_{ijkl}^{ep} is the temperature-dependent elastic-plastic constituent tensor, and $d\lambda$ is a non-negative scalar function that varies throughout the plastic loading history.

3.2.2 Concrete model

Since concrete has complex characteristics, it is difficult to define a general constitutive model to describe its material behaviour under various loading conditions. Over the years, some 3D constitutive concrete models have been developed for use at ambient temperature. At elevated temperatures, however, the constitutive model of concrete under triaxial loading is still a problem. Development of an effective constitutive model, which can represent concrete stress-strain relationships either at ambient temperature or at elevated temperature, has become a major purpose of this research. The Drucker-Prager criterion [12], which is a simple modification of the von Mises criterion, but includes the influence of hydrostatic pressure on yielding, was chosen as concrete failure function. It is expressed as

$$f(I_1, J_2) = \alpha \cdot I_1 + \sqrt{J_2} - k = 0 \tag{7}$$

where I_1 is the first invariant of the stress tensor, containing the positive material constants [13]

$$\alpha = \frac{1}{\sqrt{3}} \cdot \frac{f_c - f_t}{f_c + f_t} \tag{8}$$

$$k = \frac{2}{\sqrt{3}} \cdot \frac{f_c \cdot f_t}{f_c + f_t} \tag{9}$$

in which, f_c is the uniaxial compressive strength and f_t is the uniaxial tensile strength. At elevated temperature, the failure surface shrinks with increasing temperature along the hydrostatic axis. From Equations (8) and (9) it can be seen that α and k are functions of uniaxial strengths which are temperature-dependent. Hence, the uniaxial stress-strain relationships of concrete can be introduced into the 3D failure criterion using these material constants.

3.3 Validations

After the implementation of a 3D geometric model, material model and thermal strains into *Vulcan*, some modelling was done to validate their feasibility and accuracy. In this paper, two simulations are presented.

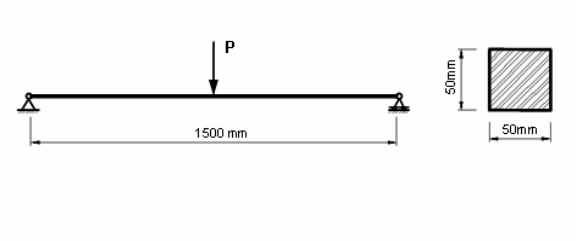

Fig. 17 – Simply supported steel beam

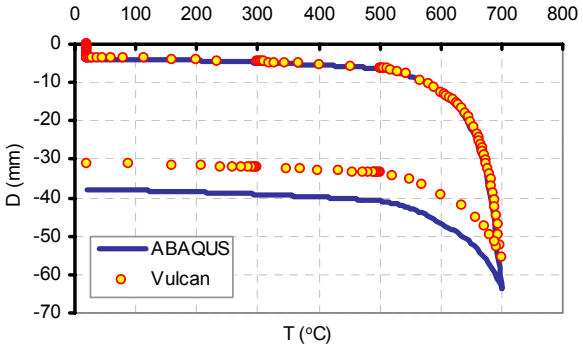

Fig. 18 – Comparisons of mid-span deflections

The first is a simply supported steel beam with 6kN concentrated load at mid-span (see Fig. 17). It is uniformly heated up to 700°C and then cooled down to 20°C. This beam was modelled by 3D brick elements within *Vulcan,* and 3D solid elements C3D8 within ABAQUS. The comparisons of deflections at mid-span are shown in Fig. 18. The trend of deformations is similar, although there is a 12% difference between the final results from *Vulcan* and ABAQUS. Moreover, before reaching 650°C, the difference is only 2% to 3% between the deflections. The reason for this could be that the plasticity models and the calculation methods for permanent strains are not identical in both programs.

In order to validate the concrete model, a concrete cube subject to different boundary conditions and thermal loads was simulated by the non-linear procedure developed. Concrete properties and loading modes are shown in Table 2. From Fig. 20, it can be seen that Case 1 failed at the uniaixal compressive strength, but Case 2 failed at an earlier stage. This is because

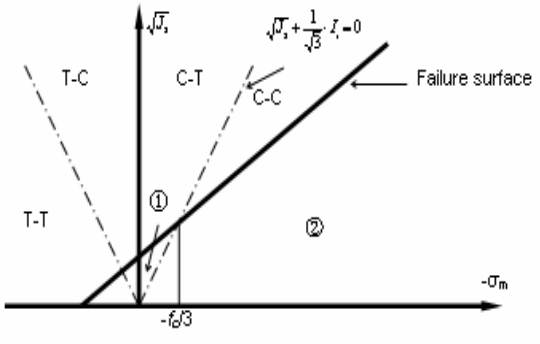

Fig. 19 – Failure zones

differential thermal expansions can induce tensile forces into the concrete, so that stress points enter into Zone ① (see Fig. 19) which is much weaker and closer to the failure surface. Cases 3 and 4 are concrete confined under compression with different heating modes. Their stress state is in Zone ②. As Fig. 21 shows, their failure strengths are dramatically increased.

Table 2 Summary of modelling information

Case number	Dimension L×W (mm)	f_c (MPa)	Test load (kN)	Load mode	Thermal mode
1	100×100	49	160	Uniaxial compression	Uniform heated
2	100×100	49	160	Uniaxial compression	With temperature gradient
3	100×100	49	160	With confinement	Uniform heated
4	100×100	49	160	With confinement	With temperature gradient

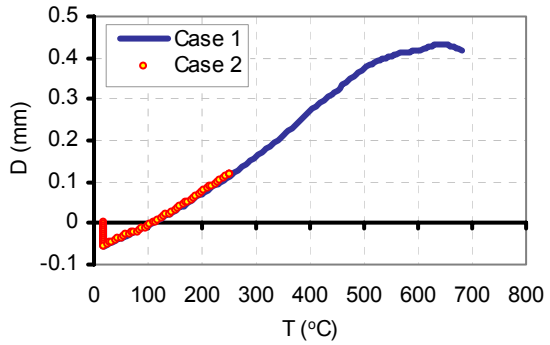

Fig. 20 – Deflection in the direction of compression

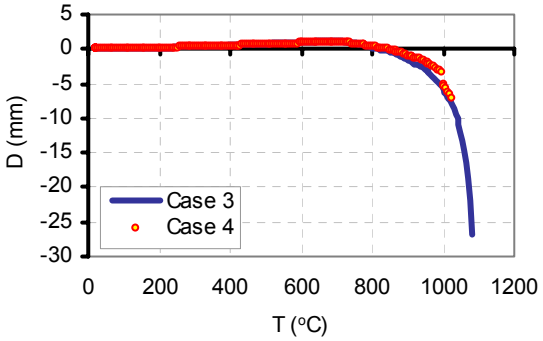

Fig. 21 – Deflection in the direction of compression

4. CONCLUSIONS

From the results of the heat transfer analyses on a Bi-Steel panel, and program validations, these points can be concluded:

1) In a Bi-Steel panel, there is a large temperature gradient from the heated steel faceplate to the cold steel faceplate. This thermal gradient could introduce large thermal stresses into the model.
2) The moisture content of concrete can affect its temperature variation significantly. The emissivity of the fire has some influence on the temperature distributions of the Bi-Steel model, but this is not significant. The steel bar connectors have a large influence on the temperature distribution, and cannot be ignored in analysis.
3) The non-linear procedure developed is capable of representing the behaviour of steel and concrete structures at elevated temperatures, and analytical results are reasonable. Some structural analyses on Bi-Steel panels in fire are currently being carried out with this procedure, and the results will be reported soon.

REFERENCES

[1] Roberts, T.M., and Dogan, O., "Fatigue of welded stud shear connectors in steel-concrete-steel sandwich beams", *J. Construct. Steel Research*, **45**, (1998) pp301-320,

[2] Corus Group Ltd, Bi-Steel Design & Construction Guide, Vol. 1-2, 1999.

[3] Clubley, S.K., Moy, S.J. and Xiao, R.Y., "Shear strength of steel-concrete-steel composite panels. Part I-testing and numerical modelling", *J. Construct. Steel Research*, **59**, (2003) pp781-794.

[4] Clubley, S.K., Moy, S.J. and Xiao, R.Y., "Shear strength of steel-concrete-steel composite panels. Part II-detailed numerical modelling of performance", *J. Construct. Steel Research*, **59**, (2003) pp795-808.

[5] Xie, M., and Chapman, J. C., "Static and fatigue tensile strength of friction-welded bar-plate connections embedded in concrete", *J. Construct. Steel Research*, **61**, (2005) pp651-673.

[6] Xie, M., Foundoukos, N. and Chapman, J.C., "Experimental and numerical investigation on the shear behaviour of friction-welded bar- plate connections embedded in concrete", *J. Construct. Steel Research*, **61**, (2005) pp625-649.

[7] EN 1991-1-2, "Eurocode 1, Actions on structures, Part 1-2: General actions-Actions on structures exposed to fire", CEN, Brussels, 2002.

[8] EN 1994-1-2, "Eurocode 4, Design of composite steel and concrete structures, Part 1-2: General rules-Structural fire design", CEN, Brussels, 2003.

[9] Gillie, M., Usmani, A., Rotter, M. and O'Connor, M., "Modelling of heated composite floor slabs with reference to the Cardington experiments", *Fire Safety Journal*, **36**, (2001) pp745-767,

[10] Huang, Z., Burgess, I.W., and Plank, R.J., "Modelling membrane action of concrete slabs in composite buildings in fire. I: Theoretical development", *Journal of Structural Engineering, ASCE*, 129(8), pp1093-1102, 2003.

[11] Bathe, K.J., "Finite Element Procedures", Prentice Hall, Englewood Cliffs, New Jersey 07632, 1996.

[12] Chen, W. F., "Constitutive Equations for Engineering Material", Vol. 2: Plasticity and Modelling, Elsevier, Amsterdam-London-New York-Tokyo, 1994.

[13] Salari, M.R., Saeb, S., Willam, K.J., Patchet, S.J., and Carrasco, R.C., "A coupled elastoplastic damage model for geomaterials", *Computer Methods in Applied Mechanics and Engineering*, **193**, (2004) pp2625-2643.